

A NUMERICAL AND EXPERIMENTAL STUDY OF A NEW DESIGN OF CLOSED DYNAMIC RESPIRATION CHAMBER

Ahmed Al Makky¹, A. Alaswad², D. Gibson³, S. Song⁴ and A. G. Olabi⁵

1. School of Engineering, University of the West of Scotland, Paisley; email: Ahmed.AIMakky@uws.ac.uk
2. School of Engineering and the Built Environment, Birmingham City University, Birmingham, England; email: Abed.Alaswad@bcu.ac.uk
3. Scottish Universities Physics Alliance, Institute of Thin Films, Sensors & Imaging email: Des.Gibson@uws.ac.uk
4. Scottish Universities Physics Alliance, Institute of Thin Films, Sensors & Imaging email: Shigeng.Song@uws.ac.uk
5. School of Engineering, University of the West of Scotland, Paisley; email: Abdul.Olabi@uws.ac.uk

Abstract

Carbon dioxide soil efflux modelling in closed dynamic respiration chambers is a challenging task. This is attributed on many occasions to the very small concentrations of carbon dioxide being transported between soil and the atmosphere. This paper describes a portable device which was made exclusively to accurately measure carbon dioxide efflux from soil locations. The blowing fan creates a forced convective flow to occur in the chamber making the K-Epsilon turbulence model a necessity to model the occurring flow in the respiration chamber gas domain. Furthermore the Darcy model is applied on the porous domain to model the flow pattern within the soil. The measurement process was achieved through measuring carbon dioxide concentration, temperature and relative humidity inside the chamber in relation to time. Simulation and experimental data is obtained using ANSYS and MATLAB. A significant agreement between the experimental and numerical results was achieved.

Keywords: Carbon Dioxide, CFD, K-Epsilon, Porous Media, Dynamic Chambers, Global Warming

32 **Roman Symbols**

A	Sample area cross section
A'	Infinitesimal planar control surface
A_n	Area of a single pore
B	Body force vector
C	Carbon dioxide constants in Sutherland equation
$C(t)$	Carbon dioxide concentration as a function of time
$\widetilde{C}(t)$	Carbon dioxide filtered concentration as a function of time
D_n	Total Integrated area for permeability function
D_{total}	Total area of pores
d_{av}	The average pore diameter for a segment of pore sizes
$H(z)$	Concentration Filter function
K	Soil permeability
K^{ij}	Area porosity tensor

K_{perm}	Permeability
K_{loss}	Empirical loss coefficient
P_k	Turbulence production
\tilde{p}	modified pressure
R^{ij}	Resistance to flow in the porous medium
r_{sand}	Sand grain diameter
r_{silt}	Silt grain diameter
r_{clay}	Clay grain diameter
T	Instance of time
\mathbf{U}	Velocity vector field
V	Studied volume of soil
V'	The volume available to flow in an infinitesimal control cell surrounding the point

33

34 - Greek Symbols

Γ_e	Effective thermal diffusivity
Γ	volume porosity

θ	Volumetric water content
M	Air dynamic viscosity
μ_e	Effective viscosity
P	Air density

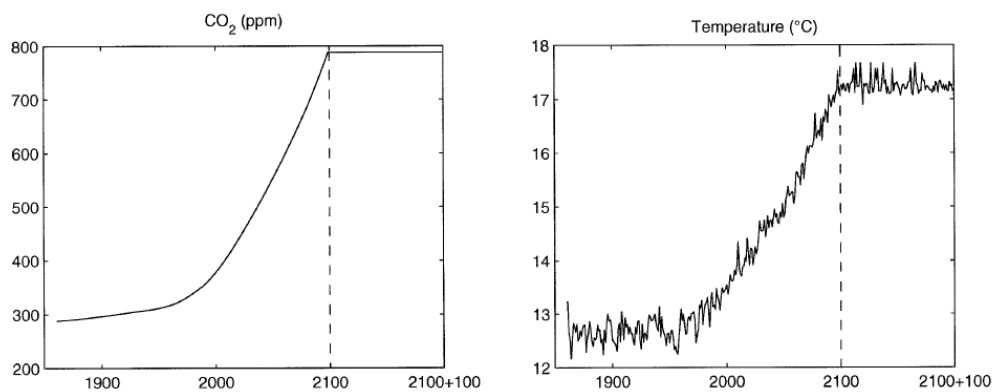
35

36

37 **1. Introduction**

38 Soil can be defined as a complex system, consisting of a mixture of organic and mineral
39 particles, soil solution and air, resulting from the interaction between biotic and abiotic factors;
40 it is the medium in which plants acquire water and nutrients through their roots system. It is
41 known by scientists that one of the physical properties of carbon dioxide contained in the
42 atmosphere is that it reflects heat back to the earth's surface. Consequently gradually the earth's
43 atmosphere traps more heat. Respiration chambers can be used to quantify the soil efflux
44 whereby they come in different shapes and sizes this depends on their application of use. They
45 are composed of two main parts; namely the chamber shell and the gas sensor. To quantify the
46 amount of produced carbon dioxide at one location, an enclosed cavity or space like a chamber
47 is used. An efflux is flowing out or forth from a porous medium (Soil) which for our case of
48 concern is carbon dioxide. Carbon dioxide gas in the soil is produced due to the biological
49 activity in the soil domain. This method was first proposed by Henrik Lundegardh in the form
50 of the respiration bell [1]. In the general context, studying respiration chambers can give
51 scientists some insight to how fertile the studied site is. That is by measuring the rate of carbon
52 dioxide produced for a certain site of concern in order to predict its impact on global warming
53 issues [2]. Consequently with the increase of carbon dioxide concentrations in the atmosphere,

54 earth responds to it [3]. Climate change is one of the most critical challenges that are facing the
55 mankind, and it is well related to the greenhouse emissions which help trapping heat and
56 making the earth warmer that affect directly weather patterns, people, plants and animals.
57 Greenhouse fluxes measurement between the soil and the atmosphere is of a great importance
58 to help to understand the biochemical parameters effects on the global warming issue. This has
59 lead scientists to use numerical nonlinear models to predict future concentrations of carbon
60 dioxide in the atmosphere [4]. Subsequently others used more sophisticated models such as the
61 dynamic global vegetation model [5] as shown in Figure 1.



62

63 **Figure 1:** IPCC IS92a projections of atmospheric CO₂ concentration and the HadCM2 SUL
64 climate model simulations of temperature over land (excluding Antarctica).
65

66 The used chamber methods have been surveyed in [6] where by it showed that new methods
67 were proposed since the early 80s with growing interest in the global warming issue, Kyoto
68 protocol. Scientists using these chambers can quantify the soil site carbon budget [7].

69 The rational for this study is to interpret and quantify for a specific location how soil produced
70 carbon dioxide contributes to the greenhouse effect. This is done by using a designed
71 respiration chamber by our research group. The main focus of this study is to use CFD
72 numerical models to show how they can assist in making the right dynamic chamber designs
73 to get the right measured fluxes representing the biological activity of location. This helps in

74 finding the right locations to install the gas sensors within the chamber and also to ensure
75 through mixing for the gas mixture. The process is firstly conducted using CAD and secondly
76 using CFD design optimization. The chamber uses a sampling tube connected with the sensor
77 hence it takes samples at all the inner chamber elevations furthermore it relies on the convective
78 flow produced by the fan to get the correct measurements instead of using a gas sensor that
79 sucks the gas sample and takes several seconds to analyse it. The selection of the blowing fan
80 location is also selected to draw out the carbon dioxide within the soil layer and at the same
81 time not to cause any disturbance to the biological activity in the soil as for cooling or
82 increasing water evaporation rates. A significant agreement between the experimental and
83 numerical results was achieved.

84 **2. Respiration Chambers**

85 Scientists know that no ideal experimental chamber exists [8], therefore the aim is always to
86 reduce measured errors. That is due to the great spatial variability in soil emissions, and to the
87 fact that the quantification of these emissions is complicated by the high spatial variability
88 exhibited by many microbial processes [9]. Respiration chambers are produced either privately
89 for research groups or by commercial companies. The transparent chamber is intended to be
90 used to measure total flux from a specific location, it is automated to ventilate the chamber,
91 while the none-transparent one is the total flux excluding the flux resulting from photosynthesis
92 process. The top hat type chamber is used for a quick site deployment where ventilation is
93 conducted manually, mostly intended for soil flux measurements. Different types of chambers
94 are available depending on the intended efflux quantity to be measured as shown in Figure 2.
95 The figure presents an example of chambers produced by the Li-Cor Inc Company with the
96 named different parts. There are four types of chambers characterised according to their
97 operational mode these are closed dynamic, open dynamic, closed static and open static
98 chambers.

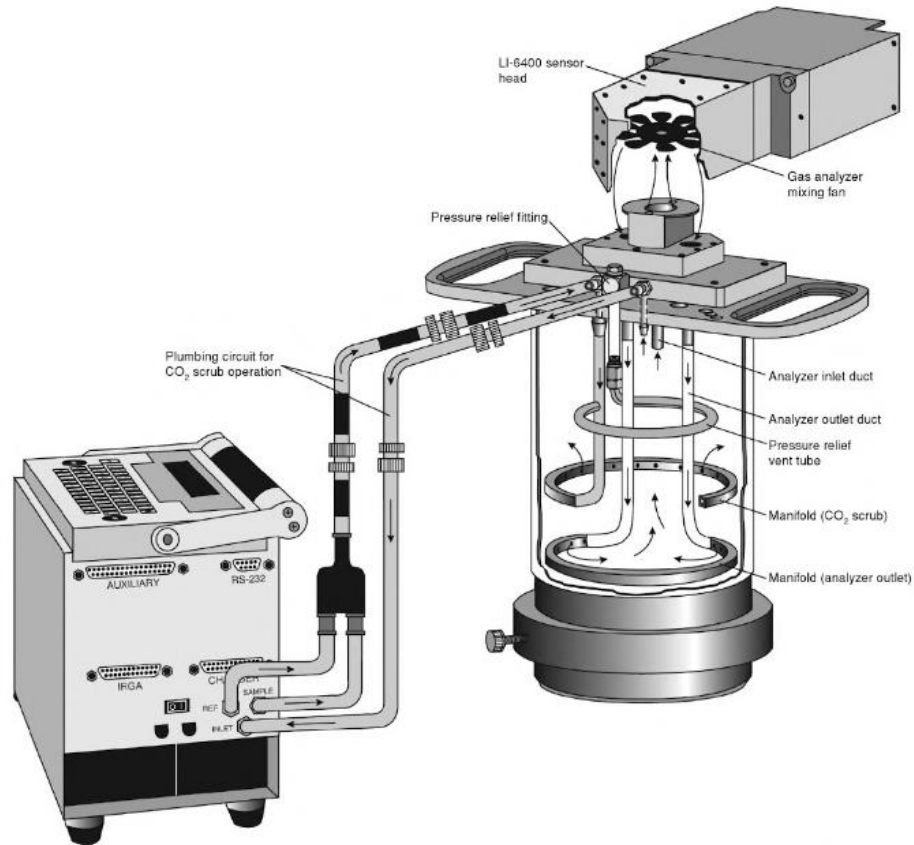


Figure 2: An example of an air circulation closed dynamic chamber made by Li-Cor Inc model (Li-cor 6400-09)[10] .

2.1. Methods of efflux Measurements

Scientists have an option to choose from several methods for measuring soil carbon dioxide efflux. These methods can be summarised into four ones, starting with the chamber soda lime [11] or what is called sometimes by alkali solution method which absorbs the respired carbon dioxide from the soil, it is an easy and cheap method to apply. The second method is by using the soil carbon dioxide gradient system method [12], generally this method is much complicated and not easy to setup. It requires the insertion of the gas sensors inside the soil layers of the studied location. This action disturbs the location integrity in addition to that gas sensors are expensive. The third method is the Eddy covariance method, sometimes referred to as micrometeorological method [13], the positive point about it that it doesn't disturb the location of study, because all the necessary sensors are attached to a tower overhead the location of study. This method can be regarded as an expensive method and represents a more

114 attractive option to measure carbon dioxide emissions from spacious locations such as
115 farmlands considering that plant community canopy emissions can also be studied taking
116 advantage of the tower setup. Finally the fourth method is by using respiration chambers that
117 use gas sensors such as infra-red gas sensors. These chambers are easy to use and setup, they
118 do introduce disturbance to the soil surface upper crust when using the chamber fixture method
119 such as the clamp method. However the cost of having several methods to choose from is the
120 large difference in accuracy, spatial and temporal resolution, and applicability. Therefore some
121 kind of compromise has to be made in the choice of (accuracy and resolution) and feasibility
122 (applicability and cost) [14]. That is why researchers have used different efflux measurement
123 methods and cross calibration functions to overcome these uncertainties [15]. The developed
124 methods can be used to validate and calibrate other classical methods used in carbon dioxide
125 measurements. The problem of under or over prediction of measured efflux, as described in
126 [16] is due to external turbulences.

127 **2.2. What is the drive behind using closed dynamic chambers?**

128 The main challenge of measuring carbon dioxide concentrations is acquiring instantaneous
129 samples every second of time. The setback in using static chambers is that the diffusion time
130 required by the carbon dioxide species to spread in a homogenous manner inside the top soil
131 crust layers and inside the chamber requires longer periods of measurements. Hence relying on
132 diffusion alone for mass transport is not practical time wise. Consequently the dynamic
133 chamber method is used for the reason that it relies on forced mass transport for the carbon
134 dioxide species. This is achieved through the use of a blowing fan inside the chamber. That
135 would decrease the required time for onsite deployment and sampling. Whereas as you move
136 down in depth from the soil surface through the soil layers mass diffusion becomes the
137 dominant factor of species transport. Hence we are interested in drawing out the gas mixture
138 of air and carbon dioxide for the specified 6 minutes of the experiment from the soil O, A and

139 B horizons. Due to that the measurement period is 6 minutes the blowing fan intention is to
140 create the suction affect to take out the stored carbon dioxide [17]. Production velocities of
141 carbon dioxide within the soil layers are in the order of 10^{-5} m/s to 10^{-7} m/s. So by sucking
142 out all the carbon dioxide stored in the O and A horizons volume the biological active has no
143 time to replenish the complete mass taken out. Hence by measuring it in 6 minutes biological
144 activity will not have enough time to produce additional carbon dioxide. This study is focused
145 mainly for closed dynamic chambers operational mode and can also be applied to static
146 chamber mode hence no venting tube is required.

147 **3. The Designed Chamber**

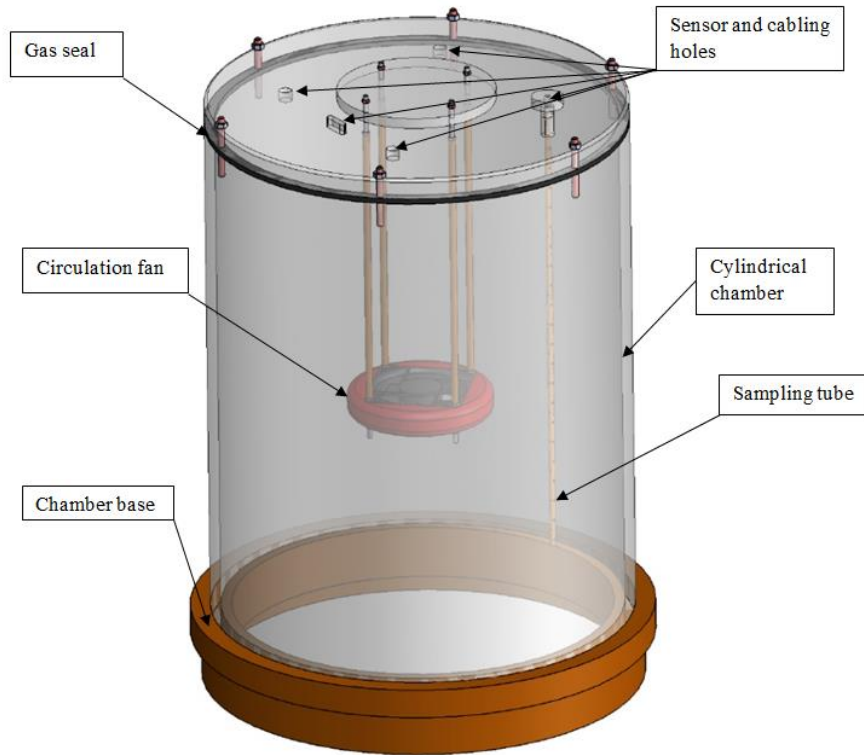
148 A chamber has been designed and made at the University of the West of Scotland (UWS),
149 sensors were fit inside it properly, which allowed experimental results to be attained.
150 Consequently, CFD numerical simulations using ANSYS (to model the fluid flow) were
151 conducted, and further experimental studies were carried out. When the chamber was designed,
152 these assumptions where made:

- 153 1- The chamber can operate in two modes the first is the steady mode (switched off fan)
154 relying on diffusive mass transport. The second mode is the unsteady mode (switched
155 on fan) relying on flow convection for mas transport, at the unsteady state the airflow
156 should sweep over the entire covered soil surface.
- 157 2- The gas efflux should be of uniform magnitude over the covered surface by the
158 chamber. The pattern of the airflow in the chamber should be relatively uniform in
159 speed across the swept soil surface. This is to create the necessary suction pressure to
160 draw out the carbon dioxide gas species from the top soil layer.
- 161 3- The fan inflow and outflow should ensure that a well-mixed air/CO₂ mixture is
162 circulated inside the chamber.

- 163 4- The diffusive flux is dominant in the steady state of operation likewise the advective
164 flow is negligible, on the contrary for the unsteady state the case is vice versa.
- 165 5- The pressure difference between the inside and outside of the chamber should be kept
166 to the minimum that is through using the chamber installation base with the soil.
- 167 6- The material for chamber fabrication should be strong to avoid possible structural
168 deformation under field conditions. A deformed chamber body may cause leakage in
169 the system and produce errors.
- 170 7- The outside surface of the chamber should be able to reflect partially solar radiation
171 [17]. Considering that each type of used chamber shell material has a predefined
172 transmissivity property.

173 Based on these assumptions, a CAD model was made as shown in Figure 3 this will be used
174 for calculating the steady-state flux. All respiration chambers have the general chamber shape
175 configuration the design contribution is evident when a comparison is conducted between
176 Figure 2 and Figure 3. For example a noted design difference is that the LICOR designs have
177 no circulation fan within them blowing in a perpendicular manner on the soil surface. The built
178 model is shown on Figure 4 installed on the grass land location where the experimental
179 measurements were taken. A general description of the experimental apparatus is that it is a
180 cylindrical transparent plastic (perspex) chamber having a height of 0.5125 m and a diameter
181 of 0.38 m. These dimensions create a chamber footprint of 0.113 m² with an internal volume
182 of 0.06 m³. It has one cap cover at the top of the chamber to allow the proper fitting of the
183 blowing fan configuration in addition to providing flexibility of distance control of the
184 convective flow intensity on the soil surface. The chamber covers a circular area of the soil.
185 During the experiment the system is placed over the soil surface at ambient temperature.

186



187

188

Figure 3: The agreed upon CAD design for the chamber to use for the study.



189

190

191

Figure 4: The used designed chamber at the University of the West of Scotland, located on the grass land site.

192 Chamber venting happens by turning over the chamber for ventilation after the measurement
193 then switching the fan on to blow out the accumulated carbon dioxide from within the chamber
194 volume. The reason for not selecting a parallel to the soil blowing fan is that blowing jet hitting
195 the chamber wall would cause a none necessary rise in internal pressure causing gas leakage
196 out of the chamber. Hence the fans distance was thoroughly selected to produce a pressure of
197 0.7 Pa. This value is equivalent to blowing winds in the range from 1 m/s to 5 m/s encountered
198 on the site location of interest this idea is discussed in [17].
199

200 **3.1 The Sensing Box**

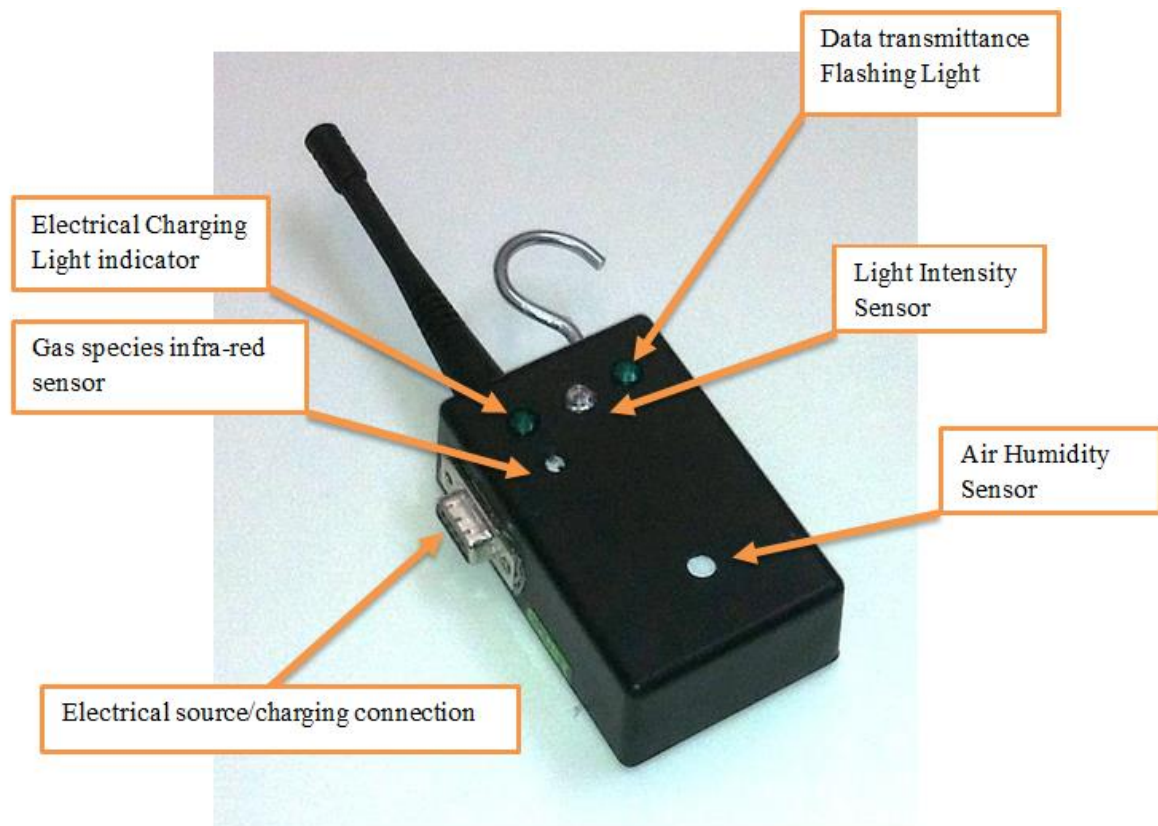
201 The sensing box as shown in Figure 5 is composed of the sensors, shown in Table 1, that are
202 connected to a microcontroller. The first one is the temperature sensor, relative humidity, Dew
203 point and light intensity. The second is the chemical species sensor which uses the non-
204 dispersive infrared gas analyzer which measures the carbon dioxide concentrations. The sensor
205 can work on battery mode while on location or can be plugged to the electrical mains for Lab
206 tests or for battery charging. The sensor box is fitted with the wireless antenna to transfer data
207 to the wireless rotor connected to the laptop. The sensing box is fitted to a sampling tube which
208 collects the data from within the chamber; the sampling tube has side holes to insure that
209 sampling is taken at the different elevations inside the chamber as shown in Figure 4. By using
210 this method a homogenous gas mixture is sampled. Meaning that better resolution
211 concentration measurement in relation to time is achieved. A precise calibration was made
212 before the experiments this was through measuring the standard atmospheric concentration of
213 carbon dioxide. The sensors sampling period was modified from 30 seconds to 5 seconds. For
214 the reason that diffusion time required 30 seconds for gas species to get to the tip of the sensor
215 in a static chamber case. The challenge was resolved through using a convective flow pattern
216 with the chamber. Pumping samples out of the chamber wasn't used because some gas sensors

217 dump the analysed gas sample into the outer environment of the chamber. The purpose of using
 218 closed chambers is to accumulate carbon dioxide concentrations within the gas volume to
 219 capture the exponential concentration curve. Gas sensors that use gas sampling technique
 220 similar to the syringe concept are not continuous because they require several seconds for the
 221 gas sample to be pumped out of the chamber and a further several seconds to conduct sample
 222 analysis. Due to using dynamic chamber and a 6 minute time measurement the issues of
 223 condensation is overcome basically because a homogenous temperature heat field is created
 224 within the chamber. The used sensor properties are summarized in Table 1, while the
 225 experimental setup and data collection steps for the dynamic chamber experiment are
 226 summarised in Figure 6.

227 **Table 1:** Technical details of the non-dispersive infrared gas analyzer.

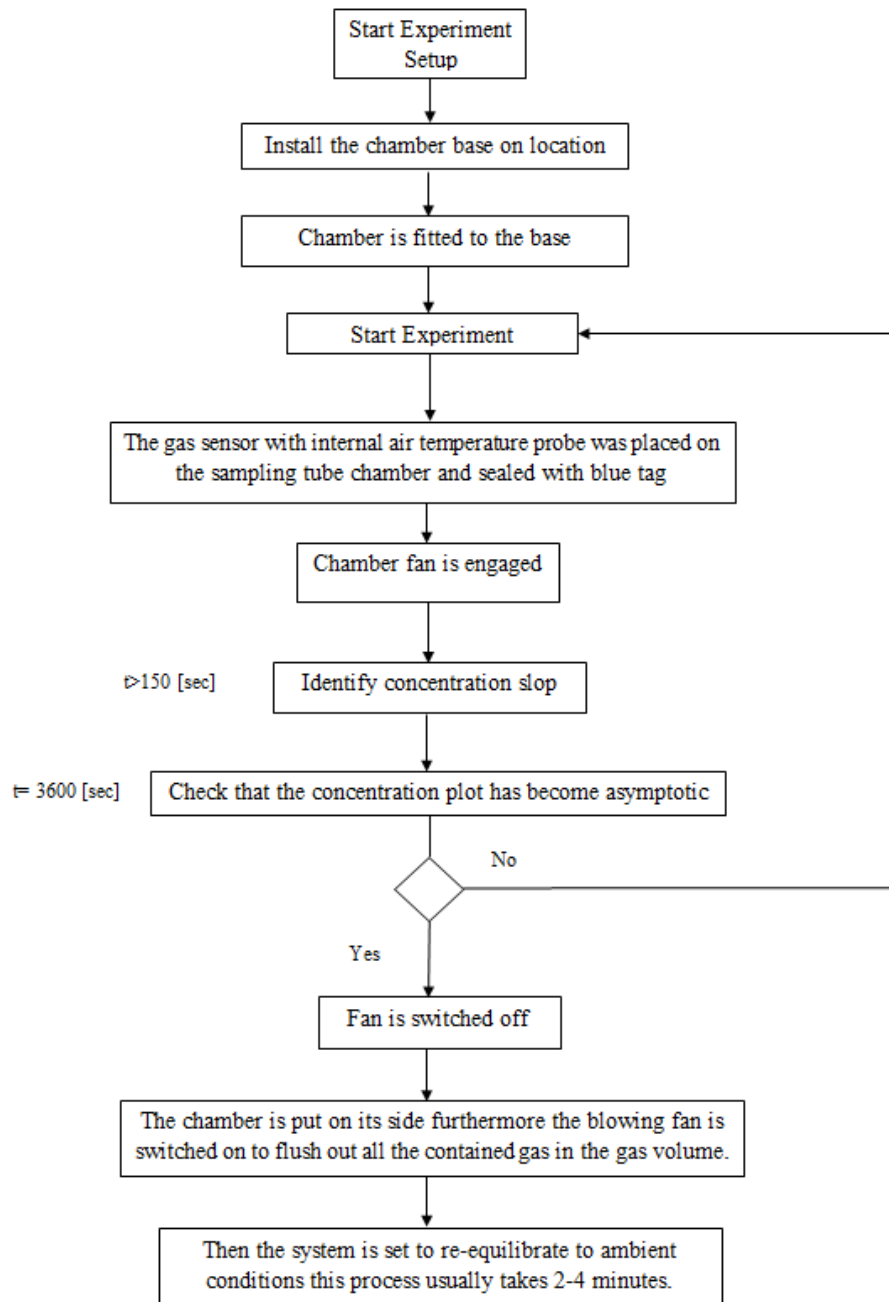
Accuracy:	+/-50ppm, or 3% of FS
Response time	<10s
Range	0-5000ppm
Working Environment	0~50°C, 0~95%RH (No water condense)
Storage temperature	-20~80°C
Power	3.5mW

228



229
230
231
232

Figure 5: The used sensor box which has the main purpose to measure carbon dioxide concentrations.



233

234

235 **Figure 6:** The flow chart showing the experimental setup steps and data collection for the
 236 dynamic chamber experiment.

237

238 3.2 Location of Study

239 Measurements were taken in Paisley which is a town located in the western part of Glasgow
 240 city. The terrain is moderately hilly near to the location as seen in Figure 7 were the location

241 has an average elevation of 15 m. Site location elevation is necessary is of importance due to
242 the relation of location height with air density. Its importance becomes apparent when
243 calculating chamber internal pressure further more in calculating chamber air mass and rate of
244 air volume recirculation in relation to time for the chamber gas volume.



245
246 **Figure 7:** Topographic map of the location of study, the site is located on University of West
247 of Scotland, the elevation key is located on the right-hand side, location is in the light green
248 colour range.

249

250 The study area is located on the prospect location tract ($55^{\circ}.50' N$, $4^{\circ}.26' W$) [18] as shown in
251 Figure 8. The selected site is a managed grassland located in the University of West Scotland
252 campus on a tended lawn surface, Sampling occurred during the days of (7th- 9th May 2015).
253 The main characteristic of the grassland site as mentioned by [19] is that it has high fertility.

254 A managed grass land is regarded as an ideal case for a studied site location hence Figure 4 is
255 used as visual proof of location of study.



256
257 **Figure 8:** The managed grass land location of study at the UWS paisley campus.

258
259 The chamber base is not permanently installed into to the location it is pushed smoothly into
260 the soil surface. But the main emphasis is to preserve the soil surface integrity as evident in
261 Figure 4. As will be evident in section 3.3 that a managed grass land location can be identified
262 on the soil texture plot shown in Figure 9 hence its porosity and permeability values can be
263 identified which are used as CFD simulation input values.

264 From experiments it was evident that for a static chamber data from the university weather
265 station is very essential for the reason that on hourly bases big temperature difference becomes
266 evident. This is attributed for that diffusion time is long especially for a chamber with a
267 relatively high headspace. While an average day time temperature measurement can be
268 satisfactory for a dynamic chamber study this is because the measurement period of 6 minutes.
269 This is for a case for acquired data from the met office. On the other hand like our case the

270 sensor box has a temperature sensor with it. The gas mixing period helps to create mainly a
271 homogenous temperature field within the chambers gas volume which showed a constant
272 temperature throughout the measurement period. The meteorological data was gathered from
273 the university weather station [20], the average measured wind speeds were 5 m/s on location.
274 The chamber sensor box measured in relation to time the following parameters: ambient
275 temperature inside the chamber was 16 C° with a dew point of 10 C° while relative humidity
276 was 40%. The importance of site description comes from the need to link climatic factors with
277 onsite measurements, because soil biological metabolism is strongly influenced by
278 temperature. Atmospheric concentrations of carbon dioxide as provided by [21] on the month
279 of May 2015 were 401ppm.

280 **3.3 Permeability Calculation**

281 There are many ways to obtain soil permeability values; its importance comes as it is an
282 essential input parameter that is needed for the numerical modelling. This parameter is an
283 essential input for the Darcy equation to model gas flow within the soil layers. Here we derive
284 a reliable method to find permeability values for a soil layer as will be shown in equation (1.5).
285 From the soil texture side experimentally the location is characterized as having a loamy sand
286 texture which can be located on Figure 9 with poor drainage with 80% sand, 15% silt and 5%
287 clay. Finding the location intrinsic permeability is based on the model of porous material made
288 up of parallel tubes of uniform sizes stated in [22] as shown in equation (1.0):

$$K = \frac{\theta}{2\pi} D_{\text{total}} \quad (1.0)$$

289 Where θ is the soil porosity, D_{total} is the total area of pores.

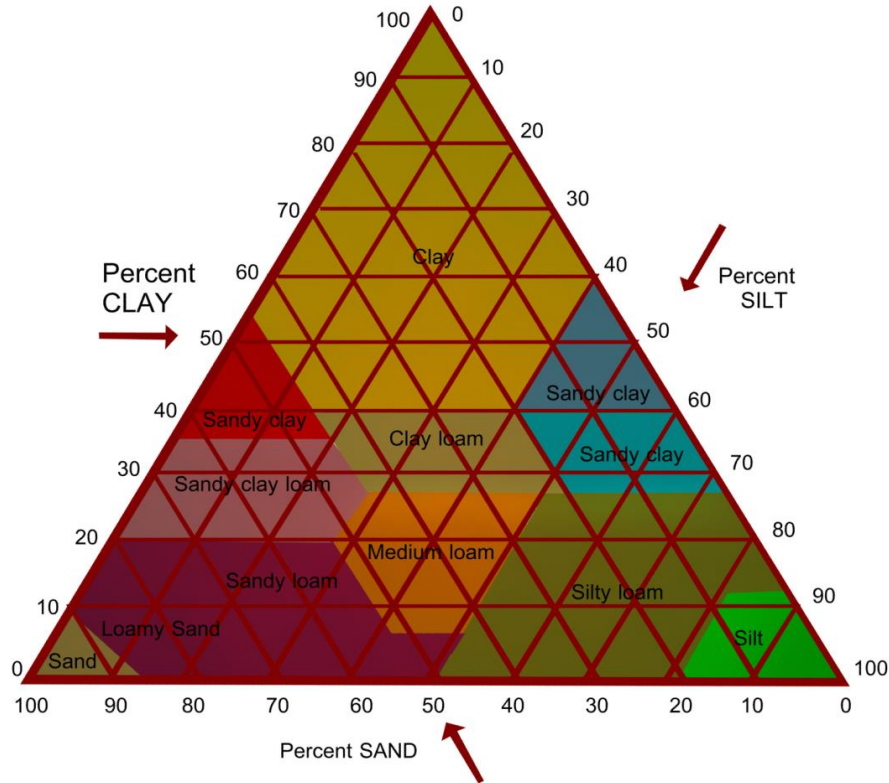


Figure 9: USDA and UK-ADAS Soil textural triangle.

To give the model the option of parallel tubes of different sizes pore size distribution is characterized using a histogram, this is later applied to equation (1.0). The area of a single pore area considered to have a circular area can be found using equation (1.1), where d_{av} is the average pore diameter for a segment of pore sizes:

$$A_n = 0.25\pi d_{av}^2 \quad (1.1)$$

Applying Newton's forward Integration law formula for two points on a single segment of the histogram, where the two points represent the minimum and maximum value of pore diameters at that segment:

$$D_n = \int_{A_n}^{A_{n+1}} r(A)dA = (A_{n+1} - A_n) \frac{r_n}{2} \quad (1.2)$$

The parameter r is the mass ratio for one of the constituents found in the soil texture triangle (example ratio of sand over total sum of constituents of sand silt and clay). By substituting

301 equation (1.1) into (1.2) the area for a segment of pore size can be calculated using equation
 302 (1.3):

$$D_n = \pi(d_{n+1}^2 - d_n^2) \frac{r_n}{8} \quad (1.3)$$

303 Equation (1.3) can be extended to different size distribution by considering macro, meso and
 304 micro pores, which for simplicity can be related to the ratios of sand, silt and clay:

$$K = \frac{\theta}{2\pi} \sum_1^{n=3} D_n = \frac{\theta}{2\pi} (D_{\text{sand}} + D_{\text{silt}} + D_{\text{clay}}) \quad (1.4)$$

305 Considering the pores diameters in equation (1.4) to be as follows for a top soil layer
 306 macropores (20 – 2000 μm), mesopores (2 – 20 μm) and micropores (0.2 – 20 μm):

$$K = \frac{\theta}{2\pi} \sum_1^{n=3} D_n = 0.25\theta((d_2^2 - d_1^2)r_{\text{sand}} + (d_3^2 - d_2^2)r_{\text{silt}} + (d_4^2 - d_3^2)r_{\text{clay}}) \quad (1.5)$$

307 In conclusion the final form takes the form shown in equation (1.6):

$$K = \frac{\theta}{2\pi} \sum_1^{n=3} D_n = 0.25\theta(a_1r_{\text{sand}} + a_2r_{\text{silt}} + a_3r_{\text{clay}}) \quad (1.6)$$

308 Where $a_1 = 10^{-6}$, $a_2 = 10^{-10}$, $a_3 = 10^{-12}$. The power of this equation is that it allows the
 309 researcher to get reasonable permeability values to be used for the simulation input based on
 310 firstly calcifying the site soil type. Consequently to later extract the ratios of sand, silt and clay
 311 from the soil texture triangle shown on Figure 9. This equation is only used to calculate
 312 permeability using the soil texture triangle. Then the researcher can find soil porosity from
 313 available literature which can assist in finding the locations water content. Depending on the
 314 soil type located on the texture triangle you can find each soil texture has different storage
 315 capacity for water according to the ratios of sand, silt and clay. These ratios have already been

316 found by scientists for grass land locations. Soil porosity for a loamy sand location (Grass land)
 317 is in the range of 0.45 to 0.47 as reported by [23] .

318 **3. 4 The K-Epsilon Turbulence Model**

319 To conduct the flow simulations ANSYS-CFX commercial software was used. The used
 320 turbulence model is the RANS model which is sometimes called K-Epsilon model [24]. The
 321 model is applied to the gas domain in the chamber, to resolve the occurring scalar field
 322 inside the chamber in relation to time. The turbulent kinetic energy K is defined as the
 323 variance of the fluctuations in velocity. This is followed by ϵ which is the turbulence Eddy
 324 dissipation, which has a dimensions of K per unit time; for example. The K-Epsilon model
 325 introduces two new variables into the system of equations. The continuity equation is equation
 326 (1.7) where ρ is the air density and \mathbf{U} is the velocity vector field:

$$\frac{\partial \rho}{\partial t} + \nabla \cdot (\rho \mathbf{U}) = 0 \quad (1.7)$$

327 The general momentum equations are:

$$\frac{\partial \rho \mathbf{U}}{\partial t} + \nabla \cdot (\rho \mathbf{U} \otimes \mathbf{U}) - \nabla \cdot (\mu_{\text{eff}} \nabla \mathbf{U}) = -\nabla \dot{p} + \nabla \cdot (\mu_{\text{eff}} \nabla \mathbf{U})^T + \mathbf{B} \quad (1.8)$$

328 Where \mathbf{B} is the sum of body forces, μ_{eff} is the effective viscosity accounting for turbulence,
 329 and \dot{p} is the modified pressure as defined in the following equation:

$$\dot{p} = p + \frac{2}{3} \rho k + \frac{2}{3} \mu_t \nabla \cdot \mathbf{U} \quad (1.9)$$

330 The model is based on the Eddy viscosity concept, so that:

$$\mu_{\text{eff}} = \mu + \mu_t \quad (1.10)$$

331 where μ_t is the turbulence viscosity. The K-Epsilon model assumes that the turbulence viscosity
 332 is linked to the turbulence kinetic energy and dissipation via the relation:

$$\mu_t = C_\mu \rho \frac{k^2}{\varepsilon} \quad (1.11)$$

333 The parameter $C_\mu = 0.09$ is $k - \varepsilon$ turbulence model constant. The values of k and ε come
 334 directly from the differential transport equations for the turbulence kinetic energy and
 335 dissipation rate:

$$\frac{\partial \rho k}{\partial t} + \nabla \cdot (\rho \mathbf{U} k) = \nabla \cdot \left(\left(\mu + \frac{\mu_t}{\sigma_k} \right) \nabla k \right) + P_k - \rho \varepsilon \quad (1.12)$$

336 In addition

$$\frac{\partial \rho \varepsilon}{\partial t} + \nabla \cdot (\rho \mathbf{U} \varepsilon) = \nabla \cdot \left(\left(\mu + \frac{\mu_t}{\sigma_\varepsilon} \right) \nabla \varepsilon \right) + \frac{\varepsilon}{k} (C_{\varepsilon 1} P_k - C_{\varepsilon 2} \rho \varepsilon) \quad (1.13)$$

337 Model used constants for (1.12) and (1.13) are taken as $C_{\varepsilon 1} = 1.44$ is, $C_{\varepsilon 2} = 1.92$, $\sigma_k = 1$ and
 338 $\sigma_\varepsilon = 1.3$. Turbulence production P_k is the due to viscous and buoyancy forces, which are
 339 modelled using equation (1.14):

$$P_k = \mu_t \nabla \mathbf{U} \cdot (\nabla \mathbf{U} + \nabla \mathbf{U}^T) - \frac{2}{3} \nabla \cdot \mathbf{U} (3\mu_t \nabla \cdot \mathbf{U} + \rho k) + P_{kb} \quad (1.14)$$

340 The average flow velocity encountered in the chamber is 2.7 m/s subsequently the flow
 341 simulation case is an incompressible flow one. Hence $\nabla \cdot \mathbf{U}$ is small and the second term on the
 342 right side of equation (1.14) does not contribute significantly to the production term. Therefore,
 343 this leads to the conclusion that there is no need to use a more sophisticated turbulence model
 344 such as LES. It is commonly known that the mentioned model requires additional
 345 computational resources to be allocated to run the calculation. The aim of using CFD
 346 simulations here is mainly to capture mass transport within the chamber and soil domain, it is
 347 not of priority to capture turbulence structures because a rotating fan wheel is not considered
 348 here.

349 3.5 Darcy Model

350 The Darcy model is derived from Reynolds transport theorem when applied to porous media.
351 This is achieved mainly by considering pressure as scalar quantity in the Reynolds transport
352 theorem. Gas exchange occurs in the studied simulation between the soil and gas medium,
353 meaning that we can rely on the theory of air movement due to pressure fluctuations [25].
354 Available in the ANSYS-CFX solver is the porous model which is at once both a generalization
355 of the Navier-Stokes equations and of Darcy's law. The main advantage of using commercial
356 software is that they come with efficient mesh generation algorithms and tools giving the user
357 the advantage of using the CFD code on complex geometries. The Darcy model [24] retains
358 both advection and diffusion terms and can therefore be used for flows in the soil domain where
359 such effects are important. In deriving the continuum equations, it is assumed that
360 'infinitesimal' control volumes and surfaces are large relative to the interstitial spacing of the
361 porous medium, but small relative to the scales that wish to resolve. Thus, from the generated
362 mesh the given control cells and control surfaces are assumed to contain both solid and fluid
363 regions. The volume porosity γ at a point is the ratio of the volume V' available to flow in an
364 infinitesimal control cell surrounding the point, and the physical volume of the cell. Hence:

$$V' = \gamma V \quad (1.15)$$

365 It is assumed that the vector area A available to flow through an infinitesimal planar control
366 surface A' is given by equation (1.16) where $K = (K^{ij})$ is called the area porosity tensor:

$$A' = K \cdot A \quad (1.16)$$

367 The dot product of a symmetric rank two tensor with a vector is:

$$K \cdot A^i = K^{ij} A_j \quad (1.17)$$

368 ANSYS CFX presently only allows K to be isotropic. The general scalar advection-diffusion
369 equation in a porous medium becomes:

$$\frac{\partial \gamma \rho \Phi}{\partial t} + \nabla \cdot (\rho \mathbf{K} \cdot \mathbf{U} \Phi) - \nabla \cdot (\Gamma \mathbf{K} \cdot \nabla \Phi) = \gamma S \quad (1.18)$$

370 In addition to the usual production and dissipation terms S will contain transfer terms from the
 371 fluid to the solid part s of the porous medium. In particular, the equation for conservation of
 372 mass:

$$\frac{\partial \gamma \rho}{\partial t} + \nabla \cdot (\rho \mathbf{K} \cdot \mathbf{U}) = 0 \quad (1.19)$$

373 And momentum is:

$$\frac{\partial \gamma \rho \mathbf{U}}{\partial t} + \nabla \cdot (\rho \mathbf{K} \cdot \mathbf{U} \otimes \mathbf{U}) - \nabla \cdot (\mu_e \mathbf{K} \cdot (\nabla \mathbf{U} + (\nabla \mathbf{U})^T)) = -\gamma \mathbf{R} \cdot \mathbf{U} + \gamma \nabla p \quad (1.20)$$

374 where \mathbf{U} is the true velocity, μ_e is the effective viscosity-either the laminar viscosity or a
 375 turbulent quantity, and $\mathbf{R} = (R^{ij})$ represents a resistance to flow in the porous medium. This is
 376 in general a symmetric positive definite second rank tensor, in order to account for possible
 377 anisotropies in the resistance. Speaking in the limit of large resistance, a large adverse pressure
 378 gradient must be set up to balance the resistance. Consequently in that limit, the two terms on
 379 the right hand side of equation (1.13) are both large and of opposite sign, and the convective
 380 and diffusive terms on the left hand side are negligible. Hence equation (1.13) reduces to:

$$\mathbf{U} = -\mathbf{R}^{-1} \cdot \nabla p \quad (1.21)$$

381 Subsequently in the limit of large resistance, we obtain an anisotropic version of Darcy's law,
 382 with the permeability kept proportional to the inverse of the resistance tensor. However, unlike
 383 Darcy's law, we are working with the actual fluid velocity components \mathbf{U} , which are
 384 discontinuous at discontinuity in porosity, rather than the continuous averaged superficial
 385 velocity:

$$\mathbf{Q} = \mathbf{K} \cdot \mathbf{U} \quad (1.22)$$

386 Heat transfer is modeled with an equation of similar form:

$$\frac{\partial \gamma \rho H}{\partial t} + \nabla \cdot (\rho \mathbf{K} \cdot \mathbf{UH}) - \nabla \cdot (\Gamma_e \mathbf{K} \cdot (\nabla H)) = \gamma S^H \quad (1.23)$$

387 Where Γ_e is an effective thermal diffusivity and S^H contains a heat source or sink to or from
 388 the porous medium. A generalized form of Darcy's law is given by

$$-\frac{\partial p}{\partial x_i} = \frac{\mu}{K_{perm}} U_i + K_{loss} \frac{\rho}{2} |\mathbf{U}| U_i \quad (1.24)$$

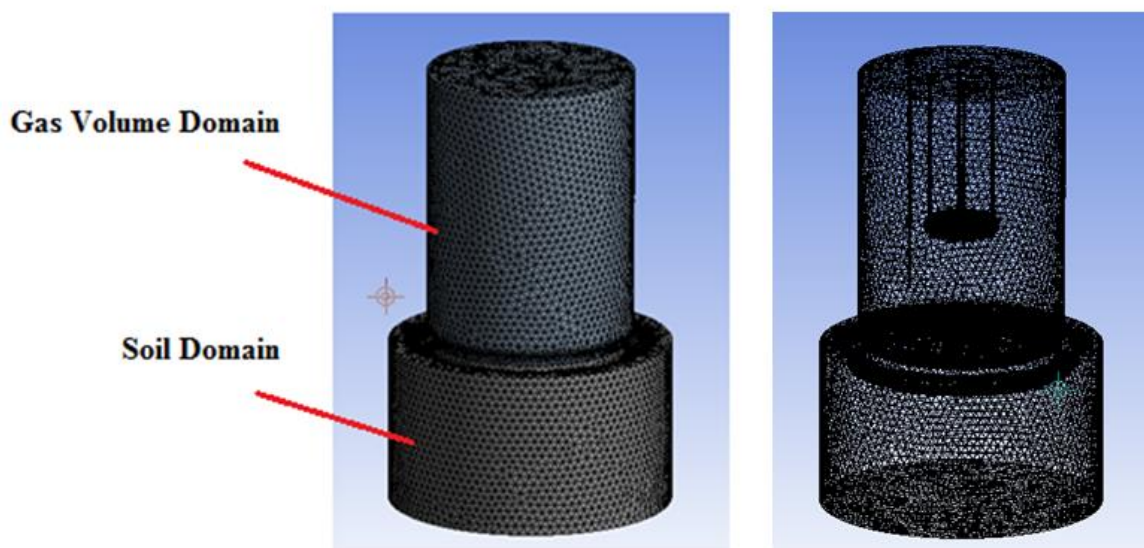
389 Therefore μ is the dynamic viscosity, K_{perm} is the permeability and K_{loss} is the empirical loss
 390 coefficient.

391 4. Numerical Analysis

392 This section is composed of the simulation setup, results and discussion.

393 4.1 Simulation Setup

394 The finite element model is composed of two domains; a porous domain representing the soil,
 395 and a gas domain representing the air Figure 10. The Navier-Stokes equations are solved to
 396 resolve the occurring flow pattern in the chamber. To model the turbulent nature of the flow,
 397 the K-Epsilon turbulence model (1.9-1.14) is applied to the Navier-Stokes equations (1.8). The
 398 Darcy equation (1.24) is solved in the porous domain to resolve the occurring flow in it. Both
 399 domains model multiple species which are air and carbon dioxide.

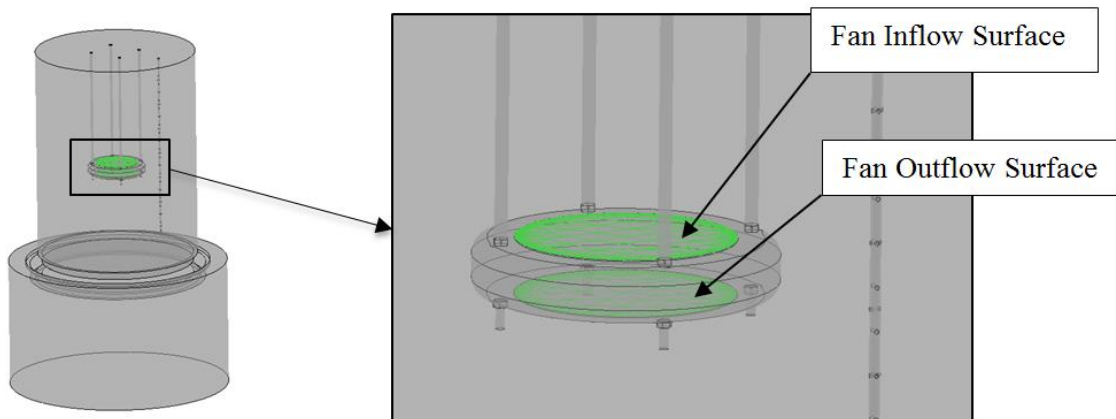


400

401 **Figure 10:** on the left the image shows the gas and porous soil domain moreover the right
402 handside image shows the generated mesh quality for both the soil and gas volume domain

403

404 To solve the mentioned equations the two domains have to be broken up into discrete elements
405 as shown on Figure 10. The tetrahedral mesh type is selected with medium size relevance centre
406 this mesh generation algorithm generates a homogenous size of elements in both domains.
407 Consequently this helps in providing volume elements that transport gas species at an instance
408 of time uniformly from the bottom of the soil domain to the tip of the gas sensor located in the
409 gas volume domain. Hence these cell volumes have a Peclet number greater than 1 for the gas
410 domain. On the contrary for the soil domain they should have a Peclet number smaller than 1.
411 The fan inflow and out flow boundary condition as shown in Figure 11 is set to 2.7 m/s while
412 all other surfaces are considered as wall boundary condition.

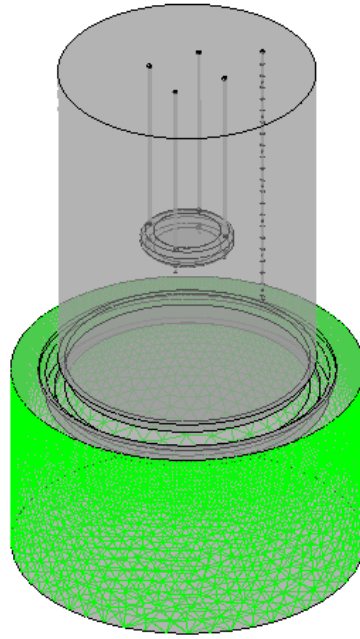


413

414 **Figure 11:** The inflow and out flow boundary surface for the fan location is highlighted in
415 green.

416

417 There are two soil surfaces for the porous media as shown in Figure 12. One is located inside
418 the chamber and the other outside the chamber. The top soil surface outside the chamber is
419 assigned an atmospheric pressure boundary condition, while inside the chamber is assigned the
420 interface boundary condition.

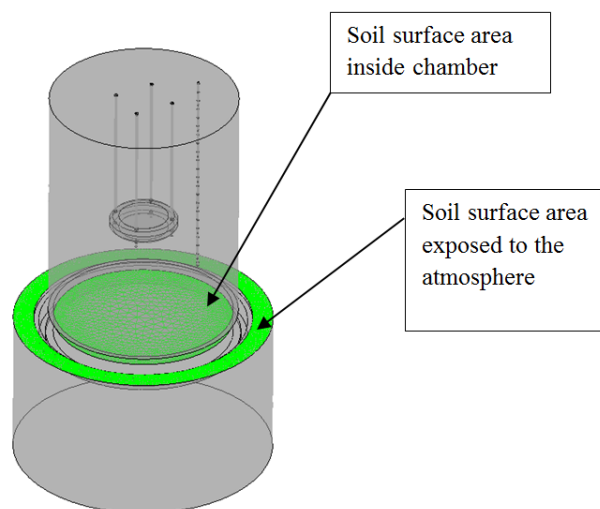


421

422 **Figure 12:** The side boundary surfaces that have been assigned an opening boundary
423 condition are laminated in light green.

424

425 The two domains are linked up using an interface boundary condition to model the mass
426 transport occurring between the both of them this is at the soil inside surface area inside
427 chamber shown in Figure 13. Gas exchange is modelled at the interface soil surface between
428 the soil and gas volume within the chamber as shown on the green surface in.



429

430 **Figure 13:** The highlighted boundary condition represents the interface boundary condition
431 between the gas volume and soil porous domain furthermore represents the boundary of the
432 porous domain with the atmosphere.

433 The carbon dioxide efflux is a result of biological activity in the soil and plants at the location.
434 To represent occurring biological activity without over complicating the project through going
435 into its chemistry the bottom surface of the porous domain is assigned a carbon dioxide source
436 term. The porous domain is assigned a 0.45 porosity based on [23]. The simulation permeability
437 value is calculated from equation (1.6) after analysing the soil sample experimentally resulting
438 10^{-10} m^2 . Both atmospheric temperature and pressure are considered to be constant with time.
439 Consequently atmospheric pressure is taken to be 1 atm and ambient temperature to be 16 C° .
440 Time stepping is conducted using first order Euler method while a time step of 1 sec is
441 considered. The total simulation time is 360 seconds, this time period is generally enough to
442 capture the gas species concentration jump which usually occurs the first 120 seconds. What
443 happens after the saturation point is that any addition of gas species doesn't contribute to any
444 addition of concentration jumps. In conclusion the concentration curve in relation to time after
445 the point of saturation becomes asymptotic. This later contributes to the numerical model
446 validation process with experimental data which as shown on Figure 16. The assigned initial
447 condition is zero velocity with a volume fraction of one for Air. So that the simulation
448 calculation starts with a pure air case for both the soil and gas domain. As the simulation
449 progresses with time carbon dioxide species disperses gradually through the two domains. The
450 simulation is run on a 16 GB RAM machine with a quad core Intel processor.

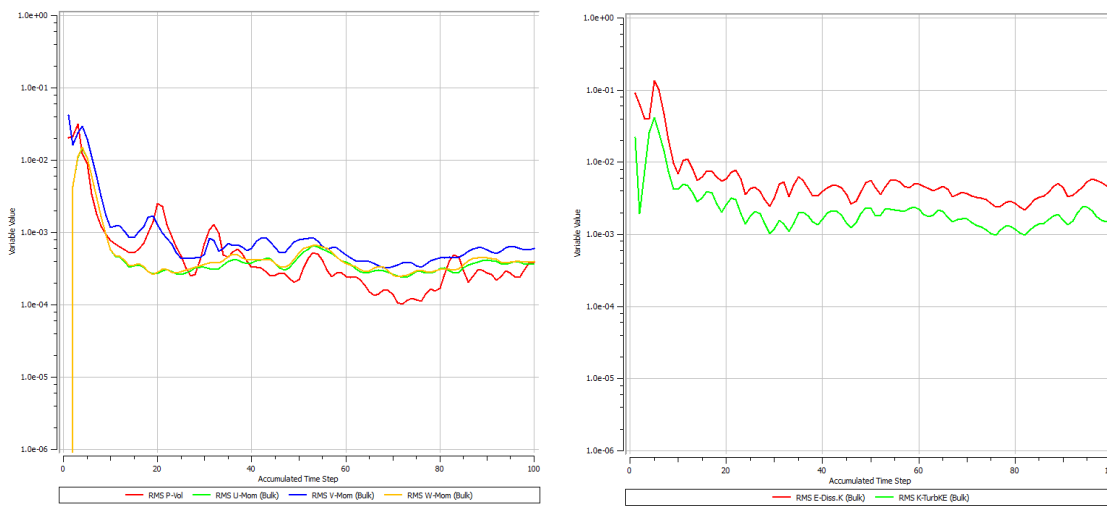
451 **4.2 Convergence check and mesh independence**

452 Looking at Figure 14 shows plots that are necessary to conduct a convergence check for the
453 conducted numerical simulation this is done for a 100 time iteration, hence due to no evident
454 jumps within the solution curves and to that they are in an order of 10^{-3} no further mesh
455 dependence is required. Moreover the left plot shows the convergence of the solution for the

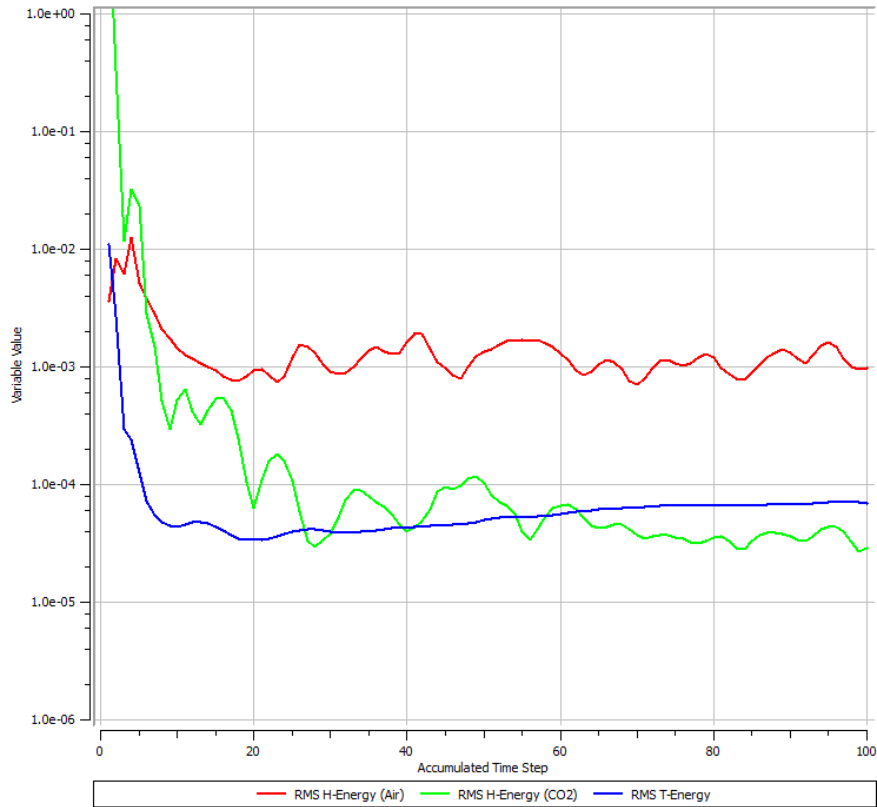
456 rms velocity components in the x y and z axis. Likewise the same is conducted for the rms
 457 pressure term. The three velocity components iterate at the same extent is due to the
 458 homogenous vector field created in the gas volume. The reason for the fluctuations with the
 459 accumulated time steps is due to the changes of flow energy inside the chamber gas volume.
 460 This is more evident on the right hand side for the convergence plot for the K-Epsilon
 461 turbulence model terms. Consequently the rms term for the kinetic energy term fluctuates and
 462 the same applies for the epsilon term which is responsible for dissipating the flow kinetic
 463 energy.

464 Furthermore commenting on Figure 15 shows a more constant iteration pattern for the rms
 465 temperature term this is attributed to a steady heat transfer rate is occurring inside the chamber.
 466 The evident noise in both rms enthalpy energy gas components is attributed to the dominance
 467 of flow convective behaviour in the gas volume.

468



469 **Figure 14:** Convergence of the solution check in relation to accumulated time step, momentum
 470 and mass solution convergence on the left and the K-Epsilon components used in the turbulence
 471 model on the right.



472

473 **Figure 15:** A convergence check of the solution for temperature in the energy equation
 474 moreover the same check for both gases enthalpy convergence.

475

476 4.3 Results and Discussion

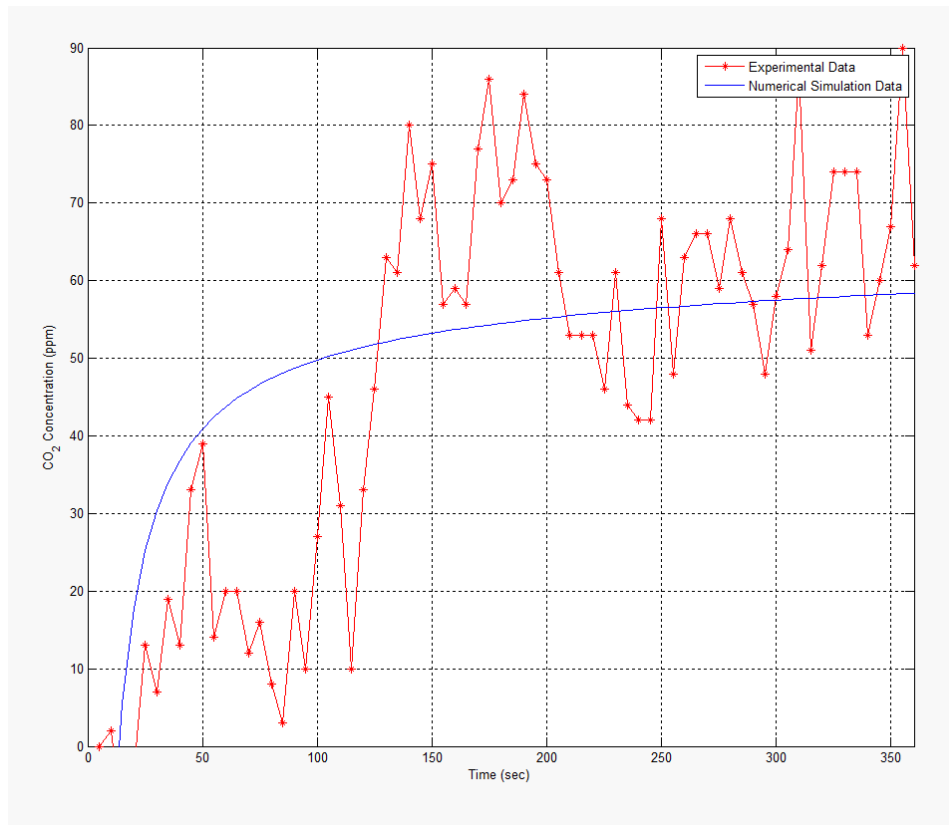
477 Figure 16 shows the experimental and flow simulation data obtained from the study. To
 478 examine the sensitivity and the frequency of the sensor sampling rate, samples initially were
 479 taken for two hours [26]. To conduct the carbon dioxide analysis, data from each 6 minute
 480 sampling period was manually analysed and the earliest 2-3 minute linear time period was used
 481 to calculate the carbon dioxide efflux in $\text{g}/\text{m}^2 \cdot \text{h}$, based on equation (1.18):

$$\bar{J}_g(t) = \frac{V \Delta C}{A \Delta t} \quad (1.18)$$

482 Where V is the chamber volume in m^3 and A is the covered soil area in m^2 , $\Delta C/\Delta t$ represents
 483 the carbon dioxide concentration derivative in relation to time mole/ m^3h . The first 150
 484 seconds time period is the necessary time to capture the flux jump that represents biological

485 activity occurring on location. By using the developed MATLAB code at UWS and analysing
486 the gathered data, this resulted in finding that the produced efflux on location is about
487 2 mole/ m²h after 150 seconds of the experiment which is a reasonable value in relation to
488 reported experimental data for a grass land location [27, 28] conducted using other types of
489 chambers. Consequently a significant agreement between the experimental readings and
490 numerical results was achieved meaning that CFD can be used to develop future respiration
491 chamber designs as shown in Figure 16. Many measurements were conducted several days
492 before the 7th of May just to confirm repeatability of experiment and the obtained data.
493 Speaking of Figure 16 it is visible from the CFD simulation, carbon dioxide concentration
494 (subtracting 400 ppm) increases gradually with the progression of time till it becomes
495 asymptotic with the experimental curve, noting that the asymptotic section of the data has been
496 cropped out. No filtering function was applied for the gathered experimental data In Figure 16
497 because dynamic chambers generate turbulence within especially for our case whereby the gas
498 sensor is plugged directly onto the chamber. From another perspective the measured
499 fluctuations are due to the interaction of the convective flow with the drilled holes in the
500 sampling tube. The transient period usually has these fluctuations in concentration but are not
501 an issue because this is due to the gas mixture reaching the sensor tip as a function of the
502 chamber turbulence. Our concern is when the measured mixture becomes asymptotic, after this
503 point, we have no concern anymore because the captured initial jump is the objective. These
504 holes purpose is to allow the mixed air carbon dioxide gas mixture to be collected and guided
505 to the sensor tip. While the numerical data in In Figure 16 shows no fluctuations this is
506 attributed to turbulence model used whereby its dissipation term is dominant. In Figure 16, a
507 gauge concentration rise (similar to gauge pressure) of 100 ppm for carbon dioxide is evident
508 during a time period of 6 minutes. The rigid limit of 100 ppm is because we are dealing with a
509 gauge concentration measurement of carbon dioxide. This is resulting from biological activity

510 within the soil and from the grass cover on location. The absolute atmospheric concentration
511 of carbon dioxide within the atmosphere can be considered as fixed and has the value of 400
512 ppm. Usually for example at a grass land soil location the gauge average measured
513 concentration is in the range of 60 ppm at the first 100 seconds of measurements.



514 **Figure 16:** An experimental and numerical representation of carbon dioxide concentration
515 with time inside the chamber.
516

517 For both curves a discrete increase in concentration exists in relation to time. The importance
518 of this curve comes in validating the obtained results. The gas concentration data in the
519 simulation is taken from the same location that the sensor is located in the experiment. This
520 ensures that correct data values are measured in relation to time and space. Sensing location is
521 of importance because sensed concentrations increase about 30 ppm between two taken
522 measurements as visible in Figure 16 for the case of experimental data at instance 80 and 90
523 sec. The deviations of measurement at every 5 seconds for the experimental data case occur
524 due to convective flow occurring within the gas volume. They are attributed to the occurring

525 turbulence in the dynamic run case. Commenting on the numerical simulation data the steady
526 behaviour is due to application of the averaging method on the scalars of the Navier Stokes
527 equations hence that omits out measurement disturbance. In conclusion the numerical model
528 shows the expected slope.

529

530 To view the process of capturing the grass land soil efflux experimentally and its challenges a
531 static case is covered in Figure 17. It is common knowledge that the atmosphere is composed
532 of many gases at different volume fractions. The measured atmospheric value of carbon dioxide
533 concentration is 402.80 ppm according to the authors in [29]. Hence to find gauge species
534 concentration values inside the chamber atmospheric values of carbon dioxide where
535 subtracted from the measurements. Consequently the gauge measured values where considered
536 which start from zero to about 120 ppm as shown in Figure 17. It is evident when looking at
537 two plotted curves that in the top figure there is lots of disturbance to the measurements;
538 therefore a MATLAB data filter is used at the bottom plot. The gauge concentration values
539 are shown in the top figure while the bottom one shows the absolute concentration after
540 applying a filtering function on it, noting that the filtered function is coloured blue furthermore
541 the unfiltered one is in red. Classically researchers in literature use exponential function with
542 one term to curve fit the disturbed set of data hence function (1.19) is obtained.

$$C(t) = 414 e^{(4e^{-6})t} \quad (1.19)$$

543 The power of using the filtering function is that it provides the initial slop to measure the
544 biological soil activity. Consequently by multiplying the function in equation (1.19) by a filter
545 $H(z)$ the general formula can be found (1.20)

$$\widetilde{C}(t) = C(t)H(z) \quad (1.20)$$

546 A MATLAB built in function is applied on the gathered dataset from the experiment this is a
 547 1-D digital filter [30]. This kind filter is used in signal analysis furthermore it can also be
 548 applied to the collected data. A moving average filter is used and is represented by equation
 549 (1.21):

$$y(n) = \frac{1}{\text{windowSize}} (x(n) + x(n - 1) + \dots + x(n - (\text{windowSize} - 1))) \quad (1.21)$$

550 Hence the numerator coefficients of the rational transfer function are defined. For the studied
 551 case it is taken as to have a value of windowSize = 30. Moreover the denominator coefficients
 552 of the rational transfer function are taken to have the value of 1. Filtering the rows or columns
 553 of the efflux matrix with the following rational transfer function (1.22):

$$H(z) = \frac{1}{1 - 0.0333 Z^{-1}} \quad (1.22)$$

554 From **Figure 17** by curve fitting the filtered function of concentration using an exponential
 555 function with one term in relation to time equation (1.23) is obtained:

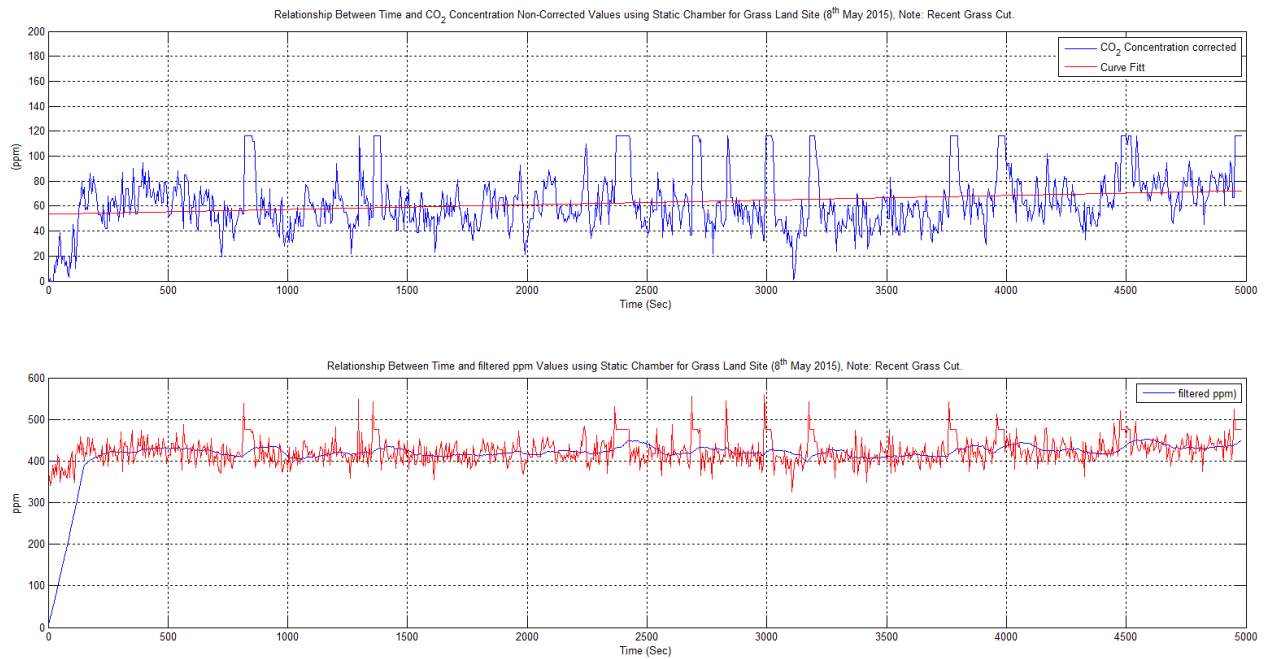
$$\widetilde{C}(t) = 391.8 e^{(2.4e^{-5})t} \quad (1.23)$$

556 What is evident when comparing equations (1.19) with (1.23) that both the filtered and
 557 unfiltered function with a one term exponential function didn't capture the exact curve hence
 558 the single term function was not considered. Furthermore an exponential function with two
 559 terms was adopted for curve fitting resulting in equation (1.24):

$$\widetilde{C}(t) = 420 e^{(3.5e^{-6})t} - 504 e^{-0.0129t} \quad (1.24)$$

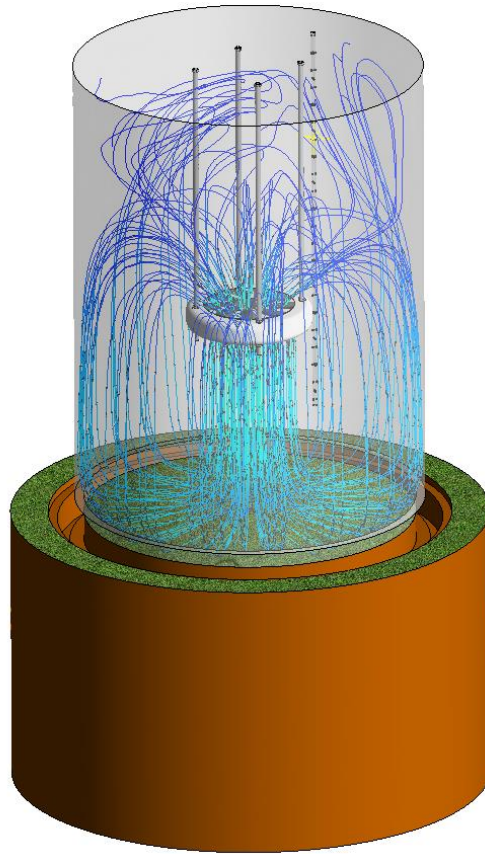
560 The extracted experimental equation is later used for the numerical simulation part of the
 561 project whereby this obtained equation is read in into the ANSYS-CFX code. Consequently it
 562 is assigned as a source term inside the biologically active soil. Without equation (1.24) it is
 563 very difficult to obtain correct results using CFD simulations. **Both data sets are correct, one**

564 captures every detail of gas diffusion in the chamber (unfiltered plot), and the other omits out
565 the diffusion disturbance (filtered).



566
567 **Figure 17:** Guage concetration top curve, absolute concentration values of measured carbon
568 dioxido measuremnts bottom (red), filtered measurments of carbon dioxoide (blue).

569
570 Speaking of Figure 18 shows the soil and fluid domains during the simulation for a dynamic
571 chamber. The soil domain is taken down to a depth of 25 cm to ensure that all the necessary
572 flow details are captured in the simulation. Looking at the chamber gas domain, the visible
573 streamlines represent the flow velocity field starting from the blowing fan outlet boundary
574 which is facing the soil surface.



575
576 **Figure 18:** Capturing the occurring flow pattern in the studied chamber using stream lines.

577
578 These stream lines hits the soil surface and travel back on a parallel path to the chamber outer
579 shell to be sucked into the fans inlet. Based on that the same mass inflow and outflow rate
580 occurs for the fan it can be considered to have periodic boundary condition. The occurring
581 circulation in the chamber is visible from the streamlines ensuring a fast homogenous mixture
582 to be established in a short period of time. Consequently this is achieved by blowing air from
583 a reasonable distance in relation to the soil surface. Hence this ensures the preservation of
584 internal chamber pressure rise to a minimum. In conclusion carbon dioxide does not leak to the
585 outside of the chamber. When the forced convective flow hits the soil surface it creates a wall
586 shear stress. This wall shear stress produces a sucking effect that draws some of the soil carbon
587 dioxide upwards instantaneously in the soil upper surface layers. The mixture is again sucked
588 from the chambers headspace by the fan producing an internal periodic flow condition. The
589 flow stream lines look symmetrical to the chambers main axis, the visible streamline

590 irregularities are due to the applied turbulence model, this is mostly evident from the suction
591 side of the fan with many twisted streamlines. Leaving the fan on for longer periods than 6
592 minutes can produce faulty fluxes due to the gradual build-up of internal pressure within the
593 chambers gas volume. The 6 minute measurement time for a dynamic chamber case is enough
594 to suck out all the stored carbon dioxide within the soil layers top layers.

595 **5. Conclusion**

596 The steps that pave the way to select and fit the right gas sensor at the right location within a
597 respiration chamber have been covered in this paper. These steps start with specifying the
598 design requirements and then proceeds to the CAD design stage. A portable device was
599 designed, made and tested. It was proven that it can be used to measure accurately carbon
600 dioxide concentration resulting from biological activity at specific locations of interest. To
601 reduce the occurrence of wrong measurements the chamber sensor takes gas samples from all
602 the elevations within the chamber using a sampling tube. Hence the sampling tube speeds up
603 the gas sample going to the sensor tip this process over takes the diffusion time that is usually
604 required for sensor measurement. This makes the sensor measurement frequency much higher
605 in resolution in relation to time. The blowing fan fitting distance from the soil surface is
606 selected thoroughly to draw out the carbon dioxide contained at the top soil biologically active
607 layers. This is based on the design condition to preserve the chambers inner pressure which
608 would contribute to any leakage out of the chamber. The researcher can to some extent rely on
609 the air viscosity properties (Energy cascade theorem) to dampen the produced kinetic energy
610 within the gas volume. CFD can contribute largely to the chamber development phase this in
611 how to use it to model producing the right gas mixture ready for measurement. This is
612 according to the experiment required sampling time, blowing fan speed and changing
613 environmental parameters from temperature, pressure, etc. This works contribution is that it

614 applied a numerical model on a gas volume and soil media to model gas exchange within a
615 respiration chamber gas volume with a blowing fan that applies a jet flow onto the soil surface.

616 The objectives of this study were achieved by running numerical tests and then through
617 comparing them with the onsite measurements using the designed chamber on the grass land
618 location. Validation of the produced data from the run simulations and apparatus showed the
619 applicability of using such an apparatus for carbon dioxide efflux measurements. The results
620 show that the K-Epsilon turbulence model can be used to model flows in the closed dynamic
621 respiration chambers. The developed numerical model can be applied to explore the occurring
622 flow patterns for different chamber designs with different soil site locations. A MATLAB
623 software can help in the data analysis stage of the project was developed. Consequently testing
624 and calibrating new sensor technologies compatibility with recently developed chamber
625 designs is applicable. The merits of using CFD tools include reductions in research costs and
626 chamber development time. CFD can predict how homogenous is a gas mixture in the chamber
627 gas volume also it can show mixing rates through visualizing the turbulence intensity and eddy
628 frequency and flow strain rates within the chamber gas volume. Hence knowing the sensors
629 frequency sampling rates and linking it with CFD can help in verifying if the sensors to be used
630 within the chamber would perform their required role or not even before making full scale
631 chamber. We can apply the different response function of concentrations for the sensor into the
632 model. CFD has its limitations also and requirements this depends on the accuracy of the
633 numerical methods used, furthermore on the generated calculation mesh and the size of the
634 finite volume elements used. This become clear especially when modelling and analysing small
635 concentration in the order of 10^{-6} or 10^{-9} .

636

637 **Acknowledgments**

638 We would like to thank the lab technicians at UWS Institute of Engineering and Energy
639 Technologies, especially Mr Robert Boyce, for their support in the practical production stage.
640 Not forgetting Mr Tom Caddell for providing the meteorological site data from the university
641 on site weather station and technical assistance on PC hardware related issues. In addition to
642 that a big thanks to Dr Torsten Howind for his long talks relating to the field of geo-mechanics.

643
644
645
646
647
648
649
650
651
652
653
654
655
656
657
658
659
660
661
662
663
664
665
666
667
668
669
670
671
672
673

674 **References**

- 675 1. Larkum, A.W.D., Contributions of Henrik Lundegårdh, in Discoveries in
676 Photosynthesis2005, Springer. p. 139-144.
- 677 2. Raich, J.W. and C.S. Potter, Global patterns of carbon dioxide emissions from soils.
678 Global Biogeochemical Cycles, 1995. **9**(1): p. 23-36.
- 679 3. Bazzaz, F.A., The response of natural ecosystems to the rising global CO₂ levels.
680 Annual review of ecology and systematics, 1990: p. 167-196.
- 681 4. Joos, F., G. Müller-Fürstenberger, and G. Stephan, Correcting the carbon cycle
682 representation: How important is it for the economics of climate change?
683 Environmental Modeling & Assessment, 1999. **4**(2-3): p. 133-140.
- 684 5. Cramer, W., et al., Global response of terrestrial ecosystem structure and function to
685 CO₂ and climate change: results from six dynamic global vegetation models. Global
686 Change Biology, 2001. **7**(4): p. 357-373.
- 687 6. Parkinson, K., An improved method for measuring soil respiration in the field. Journal
688 of Applied Ecology, 1981: p. 221-228.
- 689 7. Schlesinger, W.H. and J.A. Andrews, Soil respiration and the global carbon cycle.
690 Biogeochemistry, 2000. **48**(1): p. 7-20.
- 691 8. Widén, B. and A. Lindroth, A calibration system for soil carbon dioxide-efflux
692 measurement chambers. Soil Science Society of America Journal, 2003. **67**(1): p. 327-
693 334.
- 694 9. Roelle, P., et al., Measurement of nitrogen oxide emissions from an agricultural soil
695 with a dynamic chamber system. Journal of Geophysical Research: Atmospheres
696 (1984–2012), 1999. **104**(D1): p. 1609-1619.
- 697 10. Kutsch, W.L., M. Bahn, and A. Heinemeyer, Soil carbon dynamics: an integrated
698 methodology2009: Cambridge University Press.
- 699 11. Keith, H. and S. Wong, Measurement of soil CO₂ efflux using soda lime absorption:
700 both quantitative and reliable. Soil Biology and Biochemistry, 2006. **38**(5): p. 1121-
701 1131.
- 702 12. Maier, M. and H. Schack-Kirchner, Using the gradient method to determine soil gas
703 flux: A review. Agricultural and Forest Meteorology, 2014. **192**: p. 78-95.
- 704 13. Aubinet, M., T. Vesala, and D. Papale, Eddy covariance: a practical guide to
705 measurement and data analysis2012: Springer Science & Business Media.
- 706 14. Janssens, I.A., et al., Assessing forest soil CO₂ efflux: an in situ comparison of four
707 techniques. Tree physiology, 2000. **20**(1): p. 23-32.
- 708 15. Ngao, J., et al., Cross-calibration functions for soil CO₂ efflux measurement
709 systems. Annals of forest science, 2006. **63**(5): p. 477-484.
- 710 16. Lai, D., et al., The effect of atmospheric turbulence and chamber deployment period on
711 autochamber CO₂ and CH₄ flux measurements in an ombrotrophic peatland.
712 Biogeosciences, 2012. **9**(8): p. 3305-3322.
- 713 17. Al Makky, A., et al., Renewable energy scenario and environmental aspects of soil
714 emission measurements. Renewable and sustainable energy reviews, 2016.
- 715 18. Topographic Map Website. date of access 09/22/2015; Available from: [http://en-
716 gb.topographic-map.com/](http://en-gb.topographic-map.com/).
- 717 19. Lin, C.-J., et al., Empirical models for estimating mercury flux from soils.
718 Environmental science & technology, 2010. **44**(22): p. 8522-8528.
- 719 20. University of West of Scotland Weather Station. Available from:
720 <http://weather.uws.ac.uk/>.
- 721 21. CO₂ Monthly. 2015; Available from: <http://co2now.org/>.
- 722 22. Marshall, T.J., J.W. Holmes, and C.W. Rose, Soil physics1996: Cambridge University
723 Press.

- 724 23. Koorevaar, P., G. Menelik, and C. Dirksen, Elements of soil physics. Vol. 13. 1983:
725 Elsevier.
- 726 24. ANSYS, ANSYS CFX-Solver Modelling Guide, 2009.
- 727 25. Kimball, B. and E. Lemon, Theory of soil air movement due to pressure fluctuations.
728 Agricultural meteorology, 1972. **9**: p. 163-181.
- 729 26. Al Makky, A. et al. , A numerical and experimental study of a new design of closed
730 dyanmic respiration chambers. SEEP 2015: p. Pages 281- 286. State of the Art on
731 Environmental Protection. SEEP 2015 Conference.
- 732 27. Pumpanen, J., et al., Comparison of different chamber techniques for measuring soil
733 CO₂ efflux. Agricultural and Forest Meteorology, 2004. **123**(3): p. 159-176.
- 734 28. Fierer, N., O.A. Chadwick, and S.E. Trumbore, Production of CO₂ in soil profiles of a
735 California annual grassland. Ecosystems, 2005. **8**(4): p. 412-429.
- 736 29. CO2Now. 2016, date of access 6/1/2016; Available from: <http://co2now.org/>.
- 737 30. mathworks.1-D digital filter. Available from:
738 <http://uk.mathworks.com/help/matlab/ref/filter.html>.

739

740